Composite Structures 154 (2016) 360–373

Contents lists available at ScienceDirect

Composite Structures

journal homepage: www.elsevier.com/locate/compstruct

MITC9 shell finite elements with miscellaneous through-the-thickness functions for the analysis of laminated structures

E. Carrera [a,b], M. Cinefra [a,*], G. Li [a], G.M. Kulikov [b]

[a] Department of Aeronautics and Space Engineering, Politecnico di Torino, Turin, Italy
[b] Lab of Intelligent Materials and Structures, Tambov Technical University, Russia

ARTICLE INFO

Article history:
Received 30 June 2016
Accepted 19 July 2016
Available online 25 July 2016

Keywords:
Shell finite elements
Carrera's Unified Formulation
Sampling Surfaces method
Trigonometric
Exponential

ABSTRACT

This paper focuses on developing and exploiting the potential of miscellaneous through-the-thickness approximating functions for FEM analysis of laminated composite plates/shells. Considering the theory of series expansion, Taylor series, trigonometric series, exponential functions, and miscellaneous expansions are implemented in the equivalent single layer models of Carrera Unified Formulation (CUF). Their performances in obtaining a good approximation of stress distribution through the thickness of the plate/shell are investigated by performing several static mechanical studies, and the inclusion of Murakami's zig-zag function is also evaluated. The results are compared with layer-wise theories in the framework of CUF by adopting as thickness functions both Legendre polynomials and Lagrange interpolations on Chebyshev nodes (Sampling-Surfaces method, SaS). The governing equations are derived from Principle of Virtual Displacement (PVD) and Finite Element Method (FEM) is adopted to get the numerical solutions. Nine-node 2D elements for plates and shells are employed, using Mixed Interpolation of Tonsorial Components (MITC) method to contrast the membrane and shear locking phenomenon. Simply-supported cross-ply plate and shell structures with various lay-ups and span-to-thickness ratios subjected to transverse bi-sinusoidal pressure load are analyzed. The results show that all the refined kinematic theories are able to capture the exact solution if a sufficient number of expansion (number of terms in the expansion of the displacement field) is taken, but the maximum computational cost can change for the different types of models. In some cases, combinations of different expansion theories (miscellaneous expansions) can show a significant reduction of computational costs.

1. Introduction

Thin-walled structures like composite plates and shells play an important role in aerospace engineering. Effective mechanical models should be able to capture the elastic behaviors of multi-layered structures. Except for anisotropy, transverse shear stress calculation is an important issue for layer interfaces in laminated structures. Finite Element Method (FEM) has been widely used in engineering practice to obtain numerical approximation instead of mostly un-achievable exact analytical solutions. Given the great achievements of FEM over the past several decades in engineering application, innovative analysis methods and refined FEM models with better performances and less computational costs have been always needed.

According to published research, various theories for composite structures have been developed. They can be classified as: Equivalent Single Layer (ESL), in which the number of unknowns is independent of the number of layers, and Layer-wise approach (LW), in which the number of unknowns is dependent on the number of layers. The majority of early FEM calculations were performed with the classical Kirchhoff–Love theory and some examples are given in [1–5]. But, it was difficult to satisfy the requirements of compatibility in thin shell analysis because the rotations were derived from the transversal displacement. For this reason, plate/shell elements based on the First-order Shear Deformation Theory (FSDT) were developed by Pryor and Barker [6], Noor [7], Hughes [8], Panda and Natarayan [9], Parisch [10], Ferreira [11] and many others.

Also a large variety of plate/shell finite element implementations of higher-order theories (HOT) have been proposed in the last twenty years literature. HOT-based C^0 finite elements (C^0 means that the continuity is required only for the unknown variables and not for their derivatives) were discussed by Kant and co-authors

* Corresponding author at: Department of Aeronautics and Space Engineering, Politecnico di Torino, Corso Duca degli Abruzzi, 24, 10129 Torino, Italy.
E-mail address: maria.cinefra@polito.it (M. Cinefra).

http://dx.doi.org/10.1016/j.compstruct.2016.07.032
0263-8223/

[12,13]. In [14–18], Polit et al. proposed a C^1 six-nodes triangular finite element in which the transverse shear strains are represented by cosine functions. This element is able to ensure both the continuity conditions for displacements and transverse shear stresses at the interfaces between layers of laminated structures. A comprehensive discussion of HOT-type theories and related finite element suitability has been provided by Tessler [19]. Many other papers are available in which HOTs have been implemented for plates and shells, details can be found in the books by Reddy [20] and Palazotto and Dennis [21].

Dozens of finite elements have been proposed based on zig-zag theories [22,23]. An application of Reissner Mixed Variational Theorem (RMVT) [24] to develop standard finite elements was proposed by Rao and Meyer-Piening [25]. A generalization of RMVT as a tool to develop approximate solutions was given by Carrera [26]. The obtained finite elements represent the FE implementation of the Murakami theory [27] and were denoted by the acronym RMZC, (Reissner Mindlin Zigzag interlaminar Continuity). Full extensions of RMZC to shell geometries have been done by Brank and Carrera [28].

Concerning trigonometric polynomial expansions, some plate and beam theories have been developed. Shimpi and Ghugal [29] used trigonometric terms in the displacements field for the analysis of two layers composite beams. An ESL model was developed by Arya et al. [30] using a sine term to represent the non-linear displacement field across the thickness in symmetrically laminated beams. An extension of [30] to composite plates was presented by Ferreira et al. [31]. A trigonometric shear deformation theory is used to model symmetric composite plates discretized by a meshless method based on global multiquadric radial basis functions. A version of this theory, with a layer-wise approach, was proposed by the same authors in [32]. Vidal and Polit [33] developed a new three-noded beam finite element for the analysis of laminated beams, based on a sine distribution with layer refinement. Recently, the same authors have dealt with the influence of the Murakami's zig-zag function in the sine model for static and vibration analysis of laminated beams [34]. Static and free vibration analysis of laminated shells were performed by radial basis functions collocation, according to a sinusoidal shear deformation theory in Ferreira et al. [35]. It accounts for through-the-thickness deformation, by considering a sinusoidal evolution of all displacements along the thickness coordinate.

Concerning exponential expansions, Mantari et al. [36] presented the static response of advanced composite plates by using a new trigonometric-exponential higher order shear deformation theory (HSDT). In previous works [37–39], they demonstrated that the inclusion of exponential function in the shear strain function produces results with good accuracy. Based on this experience, they combined the exponential function with the tangential shear strain shape to obtain an improved HSDT. Karama et al. [40] developed a refined theory containing the exponential functions in thickness coordinate in the displacement field that was called as exponential shear deformation theory. In [40,41], they used this new shear stress function in the form of the exponential function to predict the mechanical behaviour of multi-layered laminated composite beams. Aydogdu [42] developed a new exponential higher order shear deformation theory for the buckling analysis of cross-ply laminated composite beams and compared the results with the theory of Karama et al. [40].

In [43,44] Carrera et al. presented the static and free vibration analysis of laminated beams using various refined beam theories by expanding the unknown displacement variables over the beam section axes using Taylor type expansions, trigonometric series, exponential, hyperbolic and zig-zag functions. A companion work [45] dealt with the analysis of laminated composite and sandwich plates by considering similar miscellaneous polynomials along the thickness direction in ESL approach. In these works, finite elements based on Carrera Unified Formulation (CUF) were used [46,47]. In the framework of CUF, a large number of refined-theories can be implemented in both ESL and LW approach for the analysis of multi-layered structures. In particular, for the analysis of the plates, MITC9 finite elements were employed [48] in which the Mixed Interpolation of Tensorial Components (MITC) method [49–52] is adopted to contrast the membrane and shear locking phenomenon. The present paper represents the extension of these elements with miscellaneous kinematics to the analysis of shell structures.

Finite element implementations of layer-wise theories were also proposed by many authors, among which Noor and Burton [53], Reddy [54], Mawenya and Davies [55], Pinsky and Kim [56], Chaudhuri and Seide [57], Rammerstorfer et al. [58]. In previous works, the authors already implemented MITC9 finite elements based on LW approach for the analysis of laminates structures and they used Legendre polynomials as thickness functions in the CUF framework [59]. In the present work, they include among the LW theories of CUF shell elements the Sampling Surface (SaS) method, introduced by Kulikov and Plotnikova [60,61] for the accurate analysis of laminated composite structures and implemented in [62] for an hybrid-mixed four-node quadrilateral laminated composite plate element (note that the origins of the SaS method can be traced back to contributions of Kulikov [63] and Kulikov and Carrera [64] in which three, four and five equally spaced SaS are employed). In this case, Lagrange polynomials are employed as thickness functions and Chebyshev polynomial nodes together with top and bottom positions of the layer are used as interpolating points along the thickness of the plate/shell.

This paper analyzes cross-ply plates and shells with simply-supported edges and subjected to transverse bi-sinusoidal pressure loads. The governing equations in weak form for the linear static analysis of composite structures are derived from the Principle of Virtual Displacement (PVD). The results, obtained with the different models, are compared with 3D exact solutions provided in literature.

The manuscript is organized as follows: an overview of ESL, ZZ and LW theories developed within the CUF framework is given in Section 2; the MITC9 shell finite element is presented in Section 1 and the constitutive relations for laminated composite structures are provided in Sections 4; in Section 5, the governing equations in weak form for the linear static analysis of composite shells are derived from the PVD. In Section 6, the results obtained using the proposed CUF theories are discussed. Section 7 is devoted to the conclusions drawn about this work.

2. Carrera Unified Formulation

The main feature of the Unified Formulation by Carrera [26] (CUF) is the unified manner in which the displacement variables are handled. In the framework of the CUF, the displacement field is written by means of approximating functions in the thickness direction as follows:

$$\delta \boldsymbol{u}^k(\alpha,\beta,z) = F_\tau(z)\delta \boldsymbol{u}^k_\tau(\alpha,\beta); \quad \boldsymbol{u}^k(\alpha,\beta,z) = F_s(z)\boldsymbol{u}^k_s(\alpha,\beta) \quad \tau,s = 0,1,\ldots,N \tag{1}$$

where (α,β,z) is a curvilinear reference system, in which α and β are orthogonal and the curvature radii R_α and R_β are constant in each point of the domain Ω (see Fig. 1). The displacement vector $\boldsymbol{u} = \{u, v, w\}$ has its components expressed in this system. $\delta\boldsymbol{u}$ indicates the virtual displacement associated to the virtual work and k identifies the layer. F_τ and F_s are the so-called thickness functions depending only on z. $\boldsymbol{u}_s$ are the unknown variables depending on the coordinates α and β. τ and s are sum indexes and N is the order

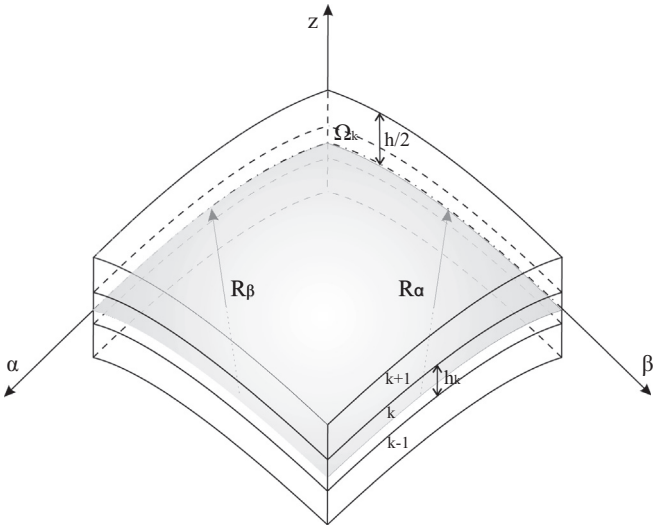

Fig. 1. Multilayered doubly-curved shell: notation and geometry.

of expansion in the thickness direction assumed for the displacements.

2.1. Equivalent Single Layer Models

2.1.1. Taylor Higher-Order Theories

In the case of Equivalent Single Layer (ESL) models, a Taylor expansion can be employed as thickness functions:

$$\boldsymbol{u} = F_0\,\boldsymbol{u}_0 + F_1\,\boldsymbol{u}_1 + \cdots + F_N\,\boldsymbol{u}_N = F_s\,\boldsymbol{u}_s, \quad s = 0, 1, \ldots, N. \tag{2}$$

$$F_0 = z^0 = 1, \quad F_1 = z^1 = z, \ \ldots, \ F_N = z^N. \tag{3}$$

Classical models, such as those based on the First-order Shear Deformation Theory (FSDT) [65], can be obtained from an ESL theory with $N = 1$, by imposing a constant transverse displacement through the thickness via penalty techniques. Also a model based on the hypotheses of Classical Lamination Theory (CLT) [66,67] can be expressed by means of the CUF by applying a penalty technique to the constitutive equations (see Section 4). This permits null transverse shear strains to be imposed in the shell.

2.1.2. Advanced Trigonometric and Exponential expansion Theories

If a trigonometric sine series plus a constant contribution is adopted, the displacement variables can be written as follows:

$$\boldsymbol{u}(\alpha,\beta,z) = \boldsymbol{u}_0(\alpha,\beta) + sin\left(\frac{\pi z}{h}\right)\boldsymbol{u}_1(\alpha,\beta) + \cdots + sin\left(\frac{n\pi z}{h}\right)\boldsymbol{u}_N(\alpha,\beta) \tag{4}$$

where h is the whole thickness dimension and n is the half-waves number. If the linear contribution is considered, the displacement expression is:

$$\boldsymbol{u}(\alpha,\beta,z) = \boldsymbol{u}_0(\alpha,\beta) + z\boldsymbol{u}_1(\alpha,\beta) + sin\left(\frac{\pi z}{h}\right)\boldsymbol{u}_2(\alpha,\beta) + \cdots + sin\left(\frac{n\pi z}{h}\right)\boldsymbol{u}_{N+1}(\alpha,\beta) \tag{5}$$

A similar description can be provided using a trigonometric cosine series:

$$\boldsymbol{u}(\alpha,\beta,z) = \boldsymbol{u}_0(x,y) + cos\left(\frac{\pi z}{h}\right)\boldsymbol{u}_1(\alpha,\beta) + \cdots + cos\left(\frac{n\pi z}{h}\right)\boldsymbol{u}_N(\alpha,\beta) \tag{6}$$

and with the linear contribution:

$$\boldsymbol{u}(x,y,z) = \boldsymbol{u}_0(\alpha,\beta) + z\boldsymbol{u}_1(\alpha,\beta) + cos\left(\frac{\pi z}{h}\right)\boldsymbol{u}_2(\alpha,\beta) + \cdots + cos\left(\frac{n\pi z}{h}\right)\boldsymbol{u}_{N+1}(\alpha,\beta) \tag{7}$$

A complete trigonometric series becomes:

$$\boldsymbol{u}(\alpha,\beta,z) = \boldsymbol{u}_0(\alpha,\beta) + sin\left(\frac{\pi z}{h}\right)\boldsymbol{u}_1(\alpha,\beta) + cos\left(\frac{\pi z}{h}\right)\boldsymbol{u}_2(\alpha,\beta) + \cdots + sin\left(\frac{n\pi z}{h}\right)\boldsymbol{u}_{2N-1}(\alpha,\beta) + cos\left(\frac{n\pi z}{h}\right)\boldsymbol{u}_{2N}(\alpha,\beta) \tag{8}$$

If the linear contribution is considered:

$$\boldsymbol{u}(\alpha,\beta,z) = \boldsymbol{u}_0(\alpha,\beta) + z\boldsymbol{u}_1(\alpha,\beta) + sin\left(\frac{\pi z}{h}\right)\boldsymbol{u}_2(\alpha,\beta) + cos\left(\frac{\pi z}{h}\right)\boldsymbol{u}_3(\alpha,\beta) + \cdots + sin\left(\frac{n\pi z}{h}\right)\boldsymbol{u}_{2N}(\alpha,\beta) + cos\left(\frac{n\pi z}{h}\right)\boldsymbol{u}_{2N+1}(\alpha,\beta) \tag{9}$$

If an exponential expansion is employed the displacement field is:

$$u(\alpha,\beta,z) = u_0(\alpha,\beta) + e^{(z/h)}\,u_1(\alpha,\beta) + \cdots + e^{(nz/h)}\,u_N(\alpha,\beta) \tag{10}$$

and adding the linear contribution:

$$u(\alpha,\beta,z) = u_0(\alpha,\beta) + z\,u_1(\alpha,\beta) + e^{(z/h)}\,u_2(\alpha,\beta) + \cdots + e^{(nz/h)}\,u_{N+1}(\alpha,\beta) \tag{11}$$

2.2. Zig-Zag Models

Due to the intrinsic anisotropy of multilayered structures, the first derivative of the displacement variables in the z-direction is discontinuous. It is possible to reproduce the zig-zag effects in the framework of the ESL description by employing the Murakami theory. According to [68], a zig-zag term can be added to the previous displacement fields as follows:

$$u = F_0\,u_0 + \cdots + F_N\,u_N + (-1)^k\zeta_k u_Z. \tag{12}$$

where $-1 < \zeta_k < 1$ is the a-dimensional thickness coordinate. Subscript Z refers to the introduced term and such theories are indicated as zig-zag (ZZ). Refined theories can be obtained by adding the zig-zag term to the Taylor polynomials expansions or the trigonometric and exponential ones.

2.3. Layer Wise Models

2.3.1. Legendre expansion

In the case of Layer-Wise (LW) models with Legendre expansion, the displacement field is defined at k-layer level as follows:

$$u^k = F_t\,u^k_t + F_b\,u^k_b + F_r\,u^k_r = F_s\,u^k_s, \qquad s = t, b, r, \quad r = 2, \ldots, N. \tag{13}$$

$$F_t = \frac{P_0 + P_1}{2}, \quad F_b = \frac{P_0 - P_1}{2}, \quad F_r = P_r - P_{r-2}. \tag{14}$$

in which $P_j = P_j(\zeta_k)$ is the Legendre polynomial of j-order defined in the ζ_k-domain: $-1 \leqslant \zeta_k \leqslant 1$. The top ($t$) and bottom ($b$) values of the displacements are used as unknown variables and one can impose the following compatibility conditions:

$$u^k_t = u^{k+1}_b, \quad k = 1, N_l - 1. \tag{15}$$

The LW models, in respect to the ESLs, allow the zig-zag form of the displacement distribution in layered structures to be modelled.

2.3.2. Sampling Surface (SaS) method

In [60] Kulikov and Plotnikova presented an efficient approach to 3D solutions of elasticity for cross-ply and angle-ply composite plates based on a new method of Sampling Surfaces (SaS). They introduced inside the nth layer an arbitrary number of SaS parallel to the middle surface, which are located at Chebyshev polynomial nodes in order to choose displacements of these surfaces as basic plate unknowns. The use of Chebyshev polynomial nodes throughout the layers can help to improve significantly the behavior of Lagrange polynomials of high degree because such choice makes it possible to minimize uniformly the error due to the Lagrange interpolation. This fact gives an opportunity to obtain the displacements and stresses with a prescribed accuracy employing the sufficiently large number of SaS. It means that the solutions based on the SaS method asymptotically approach the 3D exact solutions of elasticity as the number of SaS tends to infinity. The extension of the SaS method to 3D elasticity solutions for cylindrical and spherical laminated composite shells is given by Kulikov and Plotnikova in [61]. The work [62] presented the implementation of the SaS technique for an hybrid-mixed four-node quadrilateral laminated composite plate element. The present work implements the SaS technique for the MITC9 shell element based on the CUF [69].

According to the SaS method and Unified Formulation, the displacement field is written as:

$$u = F_0\, u_0 + F_1\, u_1 + \cdots + F_N\, u_N = F_s\, u_s, \quad s = 0, 1, \ldots, N. \tag{16}$$

where $F_s(\zeta_k)$ (thickness functions) are the Lagrange polynomials of order N given by:

$$F_s(\zeta_k) = \prod_{i=0, i\neq s}^{N} \frac{\zeta_k - \zeta_{k_i}}{\zeta_{k_s} - \zeta_{k_i}} \tag{17}$$

ζ_{k_s} are the prescribed interpolation nodes. $\zeta_{k_0} = -1$ and $\zeta_{k_N} = 1$ correspond to the top and bottom positions of the kth layer, respectively. The inner interpolating points inside the layer (for $i = 1, \ldots, N-1$) are given by the Chebyshev nodes. Indeed, they are roots of the Chebyshev polynomials of the first kind that is straightforward to minimize uniformly the error due to Lagrange interpolation [61]. This means that for a specified number $(N-1)$, the inner interpolating points of the layer., defined in the interval $(-1, 1)$, are taken as:

$$\zeta_{k_i} = cos\left(\frac{2i-1}{2(N-1)}\pi\right), \quad i = 1, 2, \ldots, N-1. \tag{18}$$

3. MITC9 shell element

In this section, the derivation of a shell finite element for the analysis of multilayered structures is presented. The element is based on both the ESL, ZZ and LW theories contained in the Unified Formulation. A nine-nodes element with exact doubly-curved geometry is considered. After an overview in scientific literature about the most efficient methods to withstand the membrane and shear locking, the MITC technique has been adopted for this element.

3.1. Geometrical relations

Shells are bi-dimensional structures in which one dimension (in general the thickness in z direction) is negligible with respect to the other two in-plane dimensions. Geometry and the reference system are indicated in Fig. 1. By considering multilayered structures, the square of an infinitesimal linear segment in the layer, the associated infinitesimal area and volume are given by:

$$\begin{aligned} ds_k^2 &= H_\alpha^{k^2}\, d\alpha_k^2 + H_\beta^{k^2}\, d\beta_k^2 + H_z^{k^2}\, dz_k^2, \\ d\Omega_k &= H_\alpha^k H_\beta^k\, d\alpha_k\, d\beta_k, \\ dV &= H_\alpha^k\, H_\beta^k\, H_z^k\, d\alpha_k\, d\beta_k\, dz_k, \end{aligned} \tag{19}$$

where the metric coefficients are:

$$H_\alpha^k = A^k(1 + z_k/R_\alpha^k), \quad H_\beta^k = B^k(1 + z_k/R_\beta^k), \quad H_z^k = 1. \tag{20}$$

k denotes the k-layer of the multilayered shell; R_α^k and R_β^k are the principal radii of the midsurface of the layer k. A^k and B^k are the coefficients of the first fundamental form of Ω_k (Γ_k is the Ω_k boundary). In this paper, the attention has been restricted to shells with constant radii of curvature (cylindrical, spherical, toroidal geometries) for which $A^k = B^k = 1$. Details for shells are reported in [70].

Geometrical relations permit the in-plane $\boldsymbol{\epsilon}_p^k$ and out-plane $\boldsymbol{\epsilon}_n^k$ strains to be expressed in terms of the displacement u. The following relations hold:

$$\begin{aligned} \boldsymbol{\epsilon}_p^k &= \left[\epsilon_{\alpha\alpha}^k, \epsilon_{\beta\beta}^k, \epsilon_{\alpha\beta}^k\right]^T = \left(D_p^k + A_p^k\right)\, u^k, \\ \boldsymbol{\epsilon}_n^k &= \left[\epsilon_{\alpha z}^k, \epsilon_{\beta z}^k, \epsilon_{zz}^k\right]^T = \left(D_{n\Omega}^k + D_{nz}^k - A_n^k\right)\, u^k. \end{aligned} \tag{21}$$

The explicit form of the introduced arrays is:

$$D_p^k = \begin{bmatrix} \frac{\partial_\alpha}{H_\alpha^k} & 0 & 0 \\ 0 & \frac{\partial_\beta}{H_\beta^k} & 0 \\ \frac{\partial_\beta}{H_\beta^k} & \frac{\partial_\alpha}{H_\alpha^k} & 0 \end{bmatrix}, \quad D_{n\Omega}^k = \begin{bmatrix} 0 & 0 & \frac{\partial_\alpha}{H_\alpha^k} \\ 0 & 0 & \frac{\partial_\beta}{H_\beta^k} \\ 0 & 0 & 0 \end{bmatrix}, \quad D_{nz}^k = \begin{bmatrix} \partial_z & 0 & 0 \\ 0 & \partial_z & 0 \\ 0 & 0 & \partial_z \end{bmatrix}, \tag{22}$$

$$A_p^k = \begin{bmatrix} 0 & 0 & \frac{1}{H_\alpha^k R_\alpha^k} \\ 0 & 0 & \frac{1}{H_\beta^k R_\beta^k} \\ 0 & 0 & 0 \end{bmatrix}, \quad A_n^k = \begin{bmatrix} \frac{1}{H_\alpha^k R_\alpha^k} & 0 & 0 \\ 0 & \frac{1}{H_\beta^k R_\beta^k} & 0 \\ 0 & 0 & 0 \end{bmatrix}. \tag{23}$$

3.2. MITC method

Considering a 9-nodes finite element, the displacement components are interpolated on the nodes of the element by means of the Lagrangian shape functions N_i:

$$\delta u_\tau = N_i \delta u_{\tau_i} \quad u_s = N_j u_{s_j} \quad \text{with} \quad i, j = 1, \ldots, 9 \tag{24}$$

where u_{s_j} and δu_{τ_i} are the nodal displacements and their virtual variations. Substituting in the geometrical relations (21) one has:

$$\begin{aligned} \boldsymbol{\epsilon}_p &= F_\tau (D_p + A_p)(N_i I) u_{\tau_i} \\ \boldsymbol{\epsilon}_n &= F_\tau (D_{n\Omega} - A_n)(N_i I) u_{\tau_i} + F_{\tau,z}(N_i I) u_{\tau_i} \end{aligned} \tag{25}$$

where I is the identity matrix.

Considering the local coordinate system (ξ, η), the MITC shell elements [71–73] are formulated by using, instead of the strain components directly computed from the displacements, an interpolation of these within each element using a specific interpolation strategy for each component. The corresponding interpolation points, called *tying points*, are shown in Fig. 2 for a nine-nodes element. Note that the transverse normal strain ϵ_{zz} is excluded from this procedure and it is directly calculated from the displacements.

The interpolating functions on the tying points are Lagrangian functions and are arranged in the following arrays:

$$\begin{aligned} N_{m1} &= [N_{A1}, N_{B1}, N_{C1}, N_{D1}, N_{E1}, N_{F1}] \\ N_{m2} &= [N_{A2}, N_{B2}, N_{C2}, N_{D2}, N_{E2}, N_{F2}] \\ N_{m3} &= [N_P, N_Q, N_R, N_S] \end{aligned} \tag{26}$$

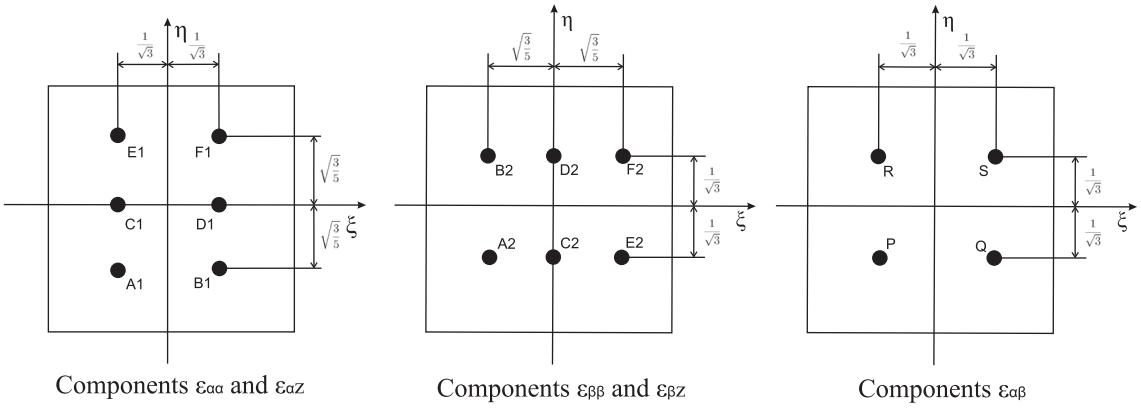

Fig. 2. Tying points for the MITC9 shell element.

From this point on, the subscripts $m1, m2$ and $m3$ indicate quantities calculated in the points $(A1, B1, C1, D1, E1, F1)$, $(A2, B2, C2, D2, E2, F2)$ and (P, Q, R, S), respectively. Therefore, the strain components are interpolated as follows:

$$\boldsymbol{\epsilon}_p = \begin{bmatrix} \epsilon_{\alpha\alpha} \\ \epsilon_{\beta\beta} \\ \epsilon_{\alpha\beta} \end{bmatrix} = \begin{bmatrix} N_{m1} & 0 & 0 \\ 0 & N_{m2} & 0 \\ 0 & 0 & N_{m3} \end{bmatrix} \begin{bmatrix} \epsilon_{\alpha\alpha_{m1}} \\ \epsilon_{\beta\beta_{m2}} \\ \epsilon_{\alpha\beta_{m3}} \end{bmatrix}$$
$$\boldsymbol{\epsilon}_n = \begin{bmatrix} \epsilon_{\alpha z} \\ \epsilon_{\beta z} \\ \epsilon_{zz} \end{bmatrix} = \begin{bmatrix} N_{m1} & 0 & 0 \\ 0 & N_{m2} & 0 \\ 0 & 0 & 1 \end{bmatrix} \begin{bmatrix} \epsilon_{\alpha z_{m1}} \\ \epsilon_{\beta z_{m2}} \\ \epsilon_{zz} \end{bmatrix} \tag{27}$$

where the strains $\epsilon_{\alpha\alpha_{m1}}, \epsilon_{\beta\beta_{m2}}, \epsilon_{\alpha\beta_{m3}}, \epsilon_{\alpha z_{m1}}, \epsilon_{\beta z_{m2}}$ are expressed by means of Eq. (25) in which the shape functions N_i and their derivatives are evaluated in the tying points. For more details about MITC method in the CUF framerwork, the reader can refer to the works [48,59,69].

4. Constitutive equations

The second step towards the governing equations is the definition of the 3D constitutive equations that permit to express the stresses by means of the strains. The generalized Hooke's law is considered, by employing a linear constitutive model for infinitesimal deformations. In a composite material, these equations are obtained in material coordinates $(1, 2, 3)$ for each orthotropic layer k and then rotated in the general curvilinear reference system (α, β, z).

Therefore, the stress–strain relations after the rotation are:

$$\begin{aligned} \boldsymbol{\sigma}_p^k &= C_{pp}^k \, \boldsymbol{\epsilon}_p^k + C_{pn}^k \, \boldsymbol{\epsilon}_n^k \\ \boldsymbol{\sigma}_n^k &= C_{np}^k \, \boldsymbol{\epsilon}_p^k + C_{nn}^k \, \boldsymbol{\epsilon}_n^k \end{aligned} \tag{28}$$

where

$$C_{pp}^k = \begin{bmatrix} C_{11}^k & C_{12}^k & C_{16}^k \\ C_{12}^k & C_{22}^k & C_{26}^k \\ C_{16}^k & C_{26}^k & C_{66}^k \end{bmatrix} \quad C_{pn}^k = \begin{bmatrix} 0 & 0 & C_{13}^k \\ 0 & 0 & C_{23}^k \\ 0 & 0 & C_{36}^k \end{bmatrix}$$
$$C_{np}^k = \begin{bmatrix} 0 & 0 & 0 \\ 0 & 0 & 0 \\ C_{13}^k & C_{23}^k & C_{36}^k \end{bmatrix} \quad C_{nn}^k = \begin{bmatrix} C_{55}^k & C_{45}^k & 0 \\ C_{45}^k & C_{44}^k & 0 \\ 0 & 0 & C_{33}^k \end{bmatrix} \tag{29}$$

The material coefficients C_{ij} depend on the Young's moduli E_1, E_2, E_3, the shear moduli G_{12}, G_{13}, G_{23} and Poisson moduli $\nu_{12}, \nu_{13}, \nu_{23}, \nu_{21}, \nu_{31}, \nu_{32}$ that characterize the layer material.

5. Governing equations

This section presents the derivation of the governing finite element stiffness matrix based on the Principle of Virtual Displacement (PVD) in the case of multi-layered doubly-curved shells subjected to mechanical loads.

The PVD for a multilayered doubly-curved shell reads:

$$\int_{\Omega_k} \int_{A_k} \left\{ \delta \boldsymbol{\epsilon}_p^{k\,T} \boldsymbol{\sigma}_p^k + \delta \boldsymbol{\epsilon}_n^{k\,T} \boldsymbol{\sigma}_n^k \right\} H_\alpha^k H_\beta^k \, d\Omega_k dz = \int_{\Omega_k} \int_{A_k} \delta u^k p^k \, H_\alpha^k H_\beta^k \, d\Omega_k dz \tag{30}$$

where Ω_k and A_k are the integration domains in the plane and in the thickness direction, respectively. The first member of the equation represents the variation of the internal work, while the second member is the external work. $p^k = p^k(\alpha, \beta, z)$ is the mechanical load applied to the structure at layer level.

Substituting the constitutive Eq. (28), the geometrical relations written via the MITC method (27) and applying the Unified Formulation (1) and the FEM approximation (24), one obtains the following governing equations:

$$\delta q_{\tau_i}^k : \; K^{k\tau sij} q_{s_j}^k = P_{\tau_i}^k \tag{31}$$

where $K^{k\tau sij}$ is a 3×3 matrix, called fundamental nucleus, and its explicit expression is given in [69]. This is the basic element from which the stiffness matrix of the whole structure is computed. The fundamental nucleus is expanded on the indexes τ and s in order to obtain the stiffness matrix of each layer. Then, the matrices of the different layers are assembled at multi-layer level depending on the considered approach, ESL or LW. $P_{\tau i}^k$ is the fundamental nucleus for the external mechanical load. For more details, the reader can refer to [46].

5.1. Acronyms

An acronym system is given here to denote the different theories. As discussed above, the kinematics can be classified into two categories: Equivalent Single Layer Model (ESL) and Layer-wise models (LW). The kinematics based on series expansions, such as Taylor, exponential and trigonometric, are used for ESL models, while kinematics based on Legendre and Lagrange (SaS) polynomials are used for LW models. For layer-wise models, *SaSn* denotes a model based on Lagrange expansion with n interpolation points ($n = N + 1$); *LGDN* denotes a model with Legendre expansion of Nth polynomial order. ESL models are indicated by the initial letter E in the acronyms and the following letters denote the different kinds of expansions. In particular, T denotes a Taylor

Table 1
Convergence study. Plate with lamination $(0^\circ/90^\circ/0^\circ)$ and thickness ratio $a/h = 100$. LW model *SaS5* is adopted.

Mesh	$\bar{u}_z$ $(\frac{a}{2},\frac{b}{2},0)$	$\bar{\sigma}_{yy}$ $(\frac{a}{2},\frac{b}{2},\frac{h}{6})$	$10\bar{\sigma}_{yz}$ $(\frac{a}{2},0,0)$	$\bar{\sigma}_{zz}$ $(\frac{a}{2},\frac{b}{2},\frac{h}{2})$
4×4	0.5077	0.2563	1.107	1.042
8×8	0.5077	0.2539	1.089	1.003
12×12	0.5077	0.2534	1.086	1.000
16×16	0.5077	0.2533	1.085	1.000
Kulikov [60]	0.5077	0.2531	1.084	1.000
Pagano [74]	0.508	0.253	1.08	1.000

series expansion, *Exp* exponential expansion, *S* and *C* sine and cosine series expansions. The number following the expansion type *n* represents the number of terms used. The constant term, that is always present in ESL models, is not counted in *n*. Therefore, *SnCn* denotes a combination of *n* sine and *n* cosine terms as well as a constant term, so the total number of expansion terms is $2n+1$. If the acronym is followed by the letter *Z*, the zig-zag term is included in the displacement field. Taking *ES2C2* and *ET1Exp2Z* as examples, they refer to the following kinematics, respectively:

$$u^k(x,y,z) = u_0^k(x,y) + sin\left(\frac{\pi z}{h}\right)u_1^k(x,y) + cos\left(\frac{\pi z}{h}\right)u_2^k(x,y) + sin\left(\frac{2\pi z}{h}\right)u_3^k(x,y) + cos\left(\frac{2\pi z}{h}\right)u_4^k(x,y) \tag{32}$$

$$u^k(x,y,z) = u_0^k(x,y) + zu_1^k(x,y) + e^{\frac{z}{h}}u_2^k(x,y) + e^{\frac{2z}{h}}u_3^k(x,y) + (-1)^k\zeta_k u_{4_z}^k \tag{33}$$

6. Numerical cases

To investigate the performance of the different models, the following benchmarks are studied:

- A three-layered cross-ply square plate with symmetric lay-up sequence $(0^\circ/90^\circ/0^\circ)$
- A two-layered cross-ply cylindrical shell with anti-symmetric lay-up sequence $(0^\circ/90^\circ)$

The results are evaluated in terms of both displacements and stresses. Numerical values are provided in the tables and through-the-thickness distributions in the figures. For the same structure, the graphs are obtained considering the in-plane positions in which the numerical values are calculated. In the tables, the total number of expansion terms N_{exp} is also provided in order to compare the computational costs of the different theories.

6.1. A three-layered cross-ply square plate with lay-up sequence $(0^\circ/90^\circ/0^\circ)$

The analysis of a three-layered cross-ply rectangular plate with stacking sequence of $(0^\circ/90^\circ/0^\circ)$ under bi-sinusoidal transverse pressure is carried out. The load is applied on the top surface of the laminated plate, which is:

$$p(x,y) = p_0 \cdot sin\left(\frac{\pi x}{a}\right)sin\left(\frac{\pi y}{b}\right) \tag{34}$$

in which $p_0 = 1$. The orthotropic plate considered has dimensions of $a = 1$ in x-direction and $b = 3$ in y-direction. Simply supported boundary conditions are imposed on its four edges. Quad elements with 9 nodes are used in the FEM analysis. The lamina mechanical properties are: $E_L = 25.0$ and $E_T = 1.0$, $G_{LT} = 0.5$ and $G_{TT} = 0.2$, $\nu_{LT} = \nu_{TT} = 0.25$. Span-to-thickness ratios of $a/h = 2, 500$ are considered. The results are given in non-dimensional form according to the following formulas:

Table 2
Plate with lamination $(0^\circ/90^\circ/0^\circ)$. Results obtained with SaS and Legendre Polynomials implemented in LW approach.

a/h	Kinematics	$\bar{u}_z$ $(\frac{a}{2},\frac{b}{2},0)$	$\bar{\sigma}_{yy}$ $(\frac{a}{2},\frac{b}{2},\frac{h}{6})$	$10\bar{\sigma}_{yz}$ $(\frac{a}{2},0,0)$	$\bar{\sigma}_{zz}$ $(\frac{a}{2},\frac{b}{2},\frac{h}{2})$	N_{exp}
2	*LGD1*	7.791	1.935	5.794	0.8787	4
	LGD4	8.165	2.296	6.690	1.004	13
	SaS3	7.911	2.218	5.732	1.035	7
	SaS5	8.165	2.296	6.690	1.004	13
	SaS7	8.166	2.296	6.683	1.000	19
	Pagano [74]	8.17	2.30	6.68	1.000	
100	*LGD1*	0.5072	0.2609	0.991	31.31	4
	LGD4	0.5077	0.2533	1.085	1.000	13
	SaS3	0.5077	0.2533	0.9904	1.065	7
	SaS4	0.5077	0.2533	1.085	1.007	10
	SaS5	0.5077	0.2533	1.085	1.000	13
	Pagano [74]	0.508	0.253	1.08	1.000	

Table 3
Thick plate (a/h = 2) with lamination $(0^\circ/90^\circ/0^\circ)$. Results obtained with various and miscellaneous expansions implemented in ESL approach.

a/h	Kinematics	$\bar{u}_z$ $(\frac{a}{2},\frac{b}{2},0)$	$\bar{\sigma}_{yy}$ $(\frac{a}{2},\frac{b}{2},\frac{h}{6})$	$10\bar{\sigma}_{yz}$ $(\frac{a}{2},0,0)$	$\bar{\sigma}_{zz}$ $(\frac{a}{2},\frac{b}{2},\frac{h}{2})$	N_{exp}
2	*FSDT*	6.616	1.783	4.888	-	
	ET1	6.616	1.783	4.888	0.5118	2
	ET3	7.784	1.932	7.027	1.089	4
	ET5	7.777	2.062	5.852	1.041	6
	ET9	8.020	2.148	5.815	0.9906	10
	ET1Z	8.027	2.188	5.512	0.5680	3
	ET3Z	7.975	1.807	6.225	1.078	5
	ET5Z	8.155	1.903	6.385	1.046	7
	ET9Z	8.160	1.888	6.712	0.9939	11
	EExp1	6.481	1.592	5.430	0.8402	2
	EExp3	7.519	1.830	6.708	1.0742	4
	EExp5	7.807	2.059	6.469	1.0103	6
	EExp8	7.871	2.163	5.610	1.0999	9
	EExp1Z	7.877	1.988	5.952	0.8813	3
	EExp3Z	7.938	1.914	5.988	1.0205	5
	EExp5Z	8.076	1.874	6.371	1.0311	7
	EExp8Z	8.149	1.749	6.649	0.9415	10
	ES1	6.343	2.036	3.274	0.0324	2
	ES3	8.015	2.139	4.950	0.5761	4
	ES5	8.297	2.227	5.892	0.6261	6
	ES1Z	7.948	2.404	5.677	0.2583	3
	ES2Z	8.088	1.604	7.095	0.4558	4
	ES5Z	8.432	1.994	6.439	0.6278	7
	ES1C1	6.045	1.954	3.618	0.3587	3
	ES3C3	7.751	2.059	5.180	0.9496	7
	ES5C5	8.023	2.170	6.151	1.000	11
	ES1C1Z	7.655	2.334	5.997	0.6156	4
	ES3C3Z	8.134	1.920	6.087	0.9832	8
	ES5C5Z	8.161	1.900	6.728	0.9935	12
	ET1Exp1Z	7.774	2.123	5.786	1.087	4
	ET1Exp3Z	7.952	1.787	6.238	1.005	6
	ET1Exp5Z	8.158	1.901	6.452	0.9909	8
	ET1S1Z	8.217	1.895	5.953	0.6179	4
	ET1S2Z	8.428	2.025	6.068	0.6297	5
	ET1S3Z	8.431	1.985	6.366	0.6288	6
	Pagano [74]	8.17	2.30	6.68	1.000	

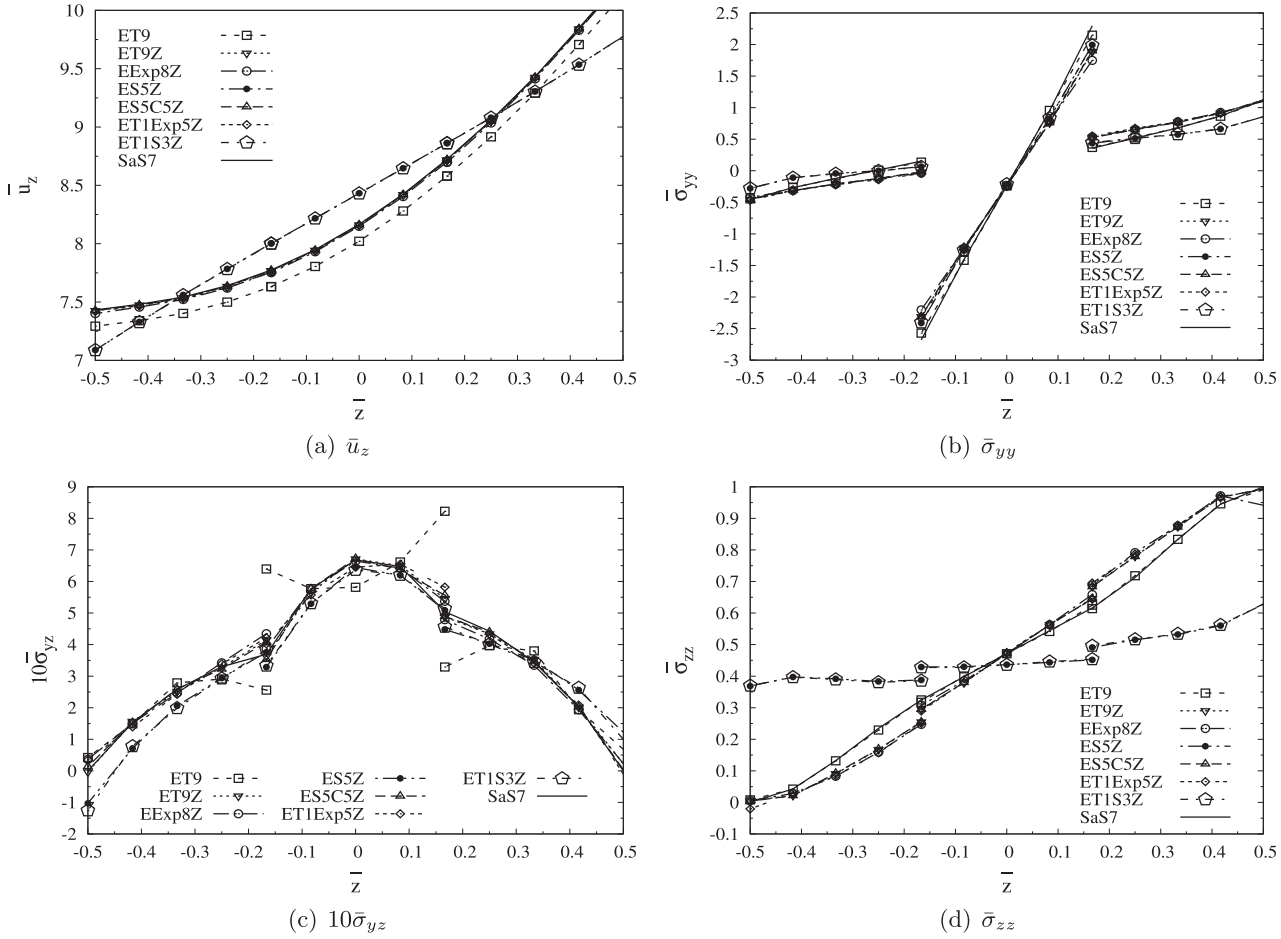

Fig. 3. Transverse displacement and stresses evaluation. Results obtained by selected kinematics, thick plate (a/h = 2).

$$\bar{u}_z = \frac{100E_T h^3}{p_0 a^4} u_z, \quad \bar{\sigma}_{xx} = \frac{h^2}{p_0 a^2}\sigma_{xx}, \quad \bar{\sigma}_{yy} = \frac{10h^2}{p_0 a^2}\sigma_{yy}, \quad \bar{\sigma}_{xy} = \frac{10h^2}{p_0 a^2}\sigma_{xy},$$
$$\bar{\sigma}_{xz} = \frac{10h}{p_0 a}\sigma_{xz}, \quad \bar{\sigma}_{yz} = \frac{10h}{p_0 a}\sigma_{yz}, \quad \bar{\sigma}_{zz} = \frac{1}{p_0}\sigma_{zz} \tag{35}$$

To reduce the computational cost, a quarter of the plate with symmetric boundary conditions is studied. Firstly, 3D stress distribution are restored with SaS (Sampling Surfaces method) [60] implemented with LW approach and the results are compared with Pagano's exact solution [74]. Then, various and miscellaneous expansions according to series expansion theories are implemented with ELS approach and their performances are tested. Results obtained with classical First Order Shear Deformation Theory (FSDT) are also listed for comparison purposes. The expansion number (number of terms in the expansion of the displacement field) is increased until convergent results and good approximation of stress distribution through the thickness are achieved. Special attention is paid to obtaining continuous transverse shear stress by including the zig-zag term.

6.1.1. Convergence and locking study

In the convergence study of Table 1, the results in terms of both displacement and stresses for $a/h = 100$ and different mesh sizes are summarized and compared with both exact solution by Pagano [74] and SaS5 analytical solution by Kulikov and Plotnikova [60]. Lagrange polynomials of order 4 (5 expansion terms) and layer-wise approach, that is SaS5 model, are used.

The convergence study demonstrates the high performance of MITC9 shell element that is stable for the analysis of thin plates and is not affected by the shear locking phenomenon. Although the mesh 8×8 provide results with acceptable accuracy, the mesh 16×16 has be chosen for the following analyses in order to ensure good convergence also for the transverse stresses.

6.1.2. Results obtained with SaS and Legendre expansions in LW approach

In Table 2, layer-wise results in terms of transversal displacement, in-plane stress and transverse shear and normal stress are given for thick and thin plates and compared with Pagano's solution [74]. Lagrange expansion on Chebyshev nodes (SaS) is compared with Legendre expansion (LGD) and it is demonstrated they provide identical results for the same polynomial order of expansion, as well as the same $N_e xp$ (compare SaS5 with LGD4). For the thick plate, more expansion terms are required to obtain very accurate results even for transverse stresses (SaS7) but acceptable results are already provided by SaS5, while for thin plate lower order models such as SaS4 and SaS5 give good approximation of both displacement and stresses.

6.1.3. Results obtained with ESL models using various and miscellaneous expansions

In Table 3, equivalent-single layer results for various and miscellaneous expansions are presented in the case of thick plate

Table 4
Thin plate (a/h = 100) with lamination (0°/90°/0°). Results obtained with various and miscellaneous expansions implemented in ESL approach.

a/h	Kinematics	$\bar{u}_z$ $(\frac{a}{2},\frac{b}{2},0)$	$\bar{\sigma}_{yy}$ $(\frac{a}{2},\frac{b}{2},\frac{h}{6})$	$10\bar{\sigma}_{yz}$ $(\frac{a}{2},0,0)$	$\bar{\sigma}_{zz}$ $(\frac{a}{2},\frac{b}{2},\frac{h}{2})$	N_{exp}
100	*FSDT*	0.5059	0.2526	1.059	–	
	*ET*1	0.5059	0.2525	1.059	91.45	2
	*ET*3	0.5071	0.2516	1.207	1.757	4
	*ET*5	0.5073	0.2520	0.9963	−0.1465	6
	*ET*1*Z*	0.5049	0.2599	1.039	91.13	3
	*ET*3*Z*	0.5077	0.2518	1.069	1.787	5
	*ET*4*Z*	0.5077	0.2521	1.069	−0.1538	6
	*EExp*1	0.02584	0.01162	11.30	6.168	2
	*EExp*3	0.4684	0.2329	−22.92	15.32	4
	*EExp*5	0.5074	0.2522	3.177	3.794	6
	*EExp*6	0.5074	0.2522	0.9608	1.915	7
	*EExp*1*Z*	0.02697	0.01254	7.629	6.119	3
	*EExp*3*Z*	0.4821	0.2392	−7.849	9.164	5
	*EExp*6*Z*	0.5076	0.2522	1.135	1.673	8
	*EExp*8*Z*	0.5077	0.2522	1.055	0.5731	10
	*ES*1	0.01079	0.006056	−9.269	1.701	2
	*ES*3	0.4497	0.2319	−34.66	81.35	4
	*ES*5	0.5050	0.2598	−0.3948	91.15	6
	*ES*1*Z*	0.02576	0.01499	−1.277	4.234	3
	*ES*3*Z*	0.4684	0.2428	−41.21	84.50	5
	*ES*5*Z*	0.5051	0.2597	0.08340	91.15	7
	*ES*8*Z*	0.5051	0.2599	1.147	91.16	10
	*ES*1*C*1	0.0108	0.0060	−9.269	0.02253	3
	*ES*3*C*3	0.4517	0.2250	−34.86	1.506	7
	*ES*5*C*5	0.5054	0.2515	8.880	−0.1700	11
	*ES*7*C*7	0.5076	0.2526	1.114	0.2924	15
	*ES*1*C*1*Z*	0.0258	0.0147	−1.280	0.7987	4
	*ES*3*C*3*Z*	0.4706	0.2357	−41.45	1.880	8
	*ES*5*C*5*Z*	0.5076	0.2523	0.0242	1.442	12
	*ES*7*C*7*Z*	0.5077	0.2525	1.029	0.2799	16
	*ET*1*Exp*1*Z*	0.5074	0.2515	0.9915	−10.61	4
	*ET*1*Exp*3*Z*	0.5077	0.2521	1.085	−1.220	6
	*ET*1*S*1*Z*	0.5051	0.2599	1.147	91.16	4
	*ET*1*S*2*Z*	0.5051	0.2599	1.129	91.16	5
	Pagano [74]	0.508	0.253	1.08	1.000	

($a/h = 2$). For completeness purposes, FSDT results are furnished. Very high expansion numbers are here required to obtain convergent results and, in the case of pure Taylor, sinusoidal or exponential expansions, they are still distant from the reference solution for both displacement and stresses. The needed expansion number is slightly reduced in the case of sinusoidal models but the results obtained are not enough accurate in respect to the reference solution. In general, it is difficult to define a general trend for exponential and sinusoidal models; some oscillation can be even noted for the exponential models (for example, in the evaluation of transverse shear stress) and the approximation of transverse stresses is very inaccurate for the sinusoidal models. For lower numbers of expansion, these last provide worse results than FSDT, even when the expansion number is comparable. In general, the inclusion of zig-zag term helps to obtain better results in terms of transverse stresses, even if the zig-zag sinusoidal models work even worse than simple sinusoidal expansion. Some benefits are given by the addition cosinusoidal terms in the trigonometric series expansions, but this implicates a considerable increase of the expansion number. By adding the linear Taylor term, the convergence is slightly improved in zig-zag exponential models and a lower expansion number is required for the convergence, while no improvements for the convergence are noted in the case of sinusoidal models. However, it is sufficient to add the T1 term in exponential and sinusoidal theories with lower number of expansion (ET1Exp1Z and ET1S1Z) to obtain very good results in respect to the FSDT solution.

Fig. 3 represents the distribution along the thickness of the transversal displacement, in-plane stress and transverse shear and normal stresses for the thick plate. For each kind of expansion, the models with highest expansion number from Tables 2 and 3 are chosen. These graphs show that good approximations are obtained with almost all kind of models with sufficient number of expansion. The pure Taylor expansion has some difficulty in satisfying the continuity conditions for the transverse stresses. If zig-zag term is not included, trigonometric and exponential expansions are not represented because they provide very inaccurate and oscillating results. As already noted in Table 3, sinusoidal models provide very inaccurate results in terms of transverse normal stress.

Similar comments can be made for the Table 4 reporting the results for the thin plate ($a/h = 100$). In this case, the order of expansion required for the convergence is lower for Taylor models, while the expansion number for the other expansions (trigonometric, exponential and miscellaneous) is almost the same of the thick plate. Most of the models don't provide accurate values in terms of transverse stresses, in particular the transverse normal stress, and very oscillating behaviors can be observed (note that in the case of thin structures the transverse stresses tend to be very small and it can be difficult to numerically approximate them). On the other hand, all the models furnish good results in terms of transversal displacement and in-plane stress. Here, the zig-zag term improves the results even for the sinusoidal models. Unlike the thick plate, the inclusion of linear Taylor term here produces some benefits in terms of convergence also for the sinusoidal model but only for the shear stress, not for the normal stress.

Fig. 4 represents the distribution along the thickness of transversal displacement, in-plane stress and transverse shear and normal stress for the thin plate. For each kind of expansion, the models with highest expansion number from Tables 2 and 4 are chosen. Similar comments to the thick plate can be made. The pure Taylor expansion has difficulty in satisfying the continuity conditions for the transverse stresses and the sinusoidal models provide very inaccurate results in terms of transverse normal stress. From Fig. 4(c), note that some models such as ES5Z, EExp6Z and ES5C5Z show very oscillating behaviors even if they provide acceptable numerical results in Table 4, therefore they have been substituted with ES8Z, EExp8Z and ES7C7Z in Fig. 4(d). The Fig. 4(e) demonstrates once again that all the models fail in the description of the transverse normal stress.

6.2. A two-layered cylindrical shell with lay-up sequence (0°/90°)

This case refers to the work of Kulikov and Plotnikova [61] and the exact solution derived by Varadan and Bhaskar [75] for the structure shown in Fig. 5.

The simply-supported circular cylindrical shell of radius R_β ($R_\alpha = \infty$) is subjected to a bi-sinusoidal distributed transverse load acting on the bottom surface:

$$p(\alpha,\beta) = -p_0 \cdot sin\left(\frac{\pi\alpha}{L}\right) sin\left(\frac{8\pi\beta}{b}\right) \tag{36}$$

where $L = 4R_\beta$ is the length of the shell and $b = 2\pi R_\beta$ is the circumference of the midsurface. The mechanical properties of the lamina are: $E_L = 25.0$ and $E_T = E_3 = 1.0$, $G_{LT} = 0.5$ and $G_{TT} = 0.2$, $\nu_{LT} = \nu_{TT} = 0.25$. Span-to-thickness ratios of $a/h = 2, 100$ are considered. To compare the results with Varadan and Bhaskar's solution [75], the following dimensionless parameters are adopted:

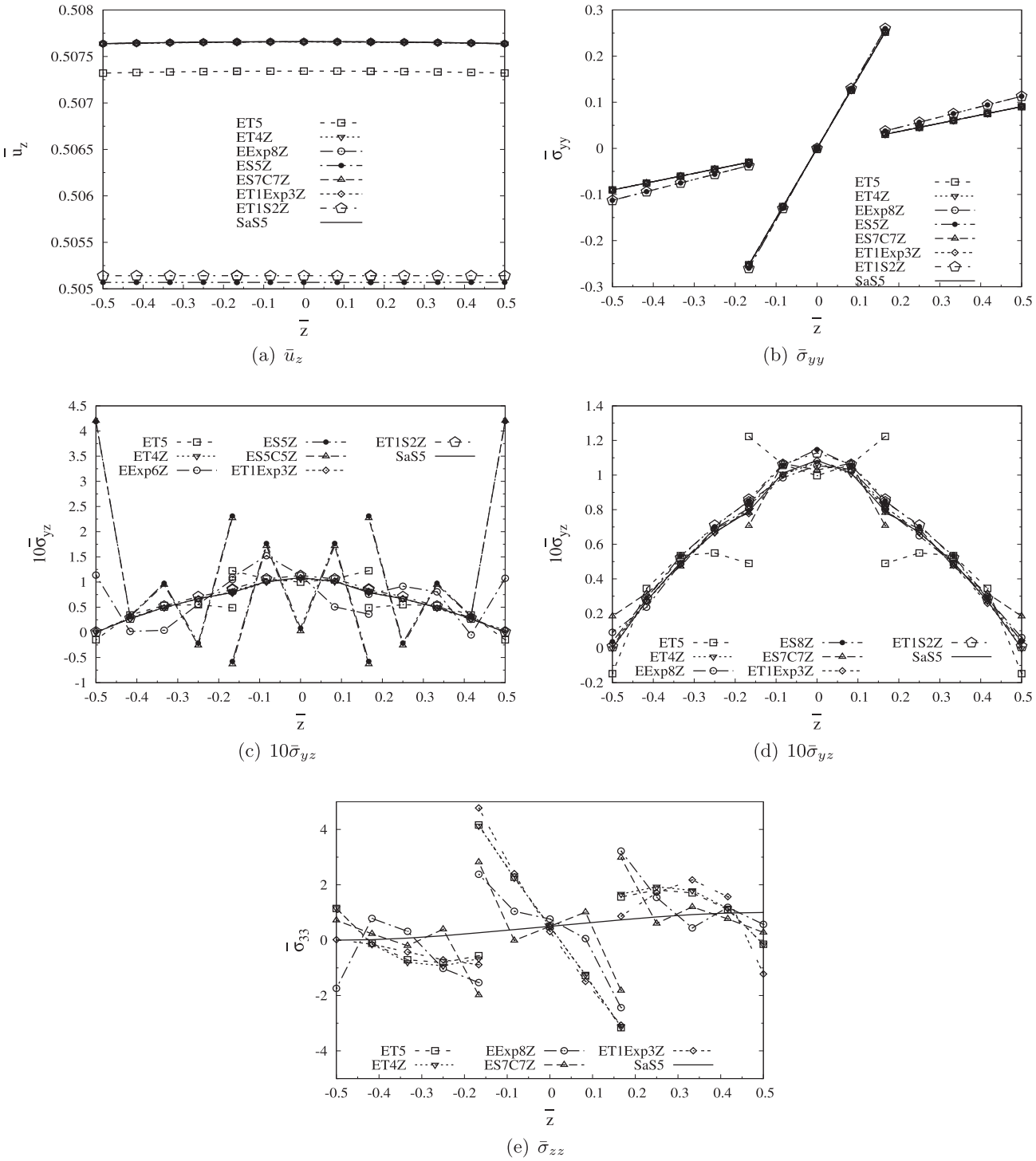

Fig. 4. Transverse displacement and stresses evaluation. Results obtained by selected kinematics, thin plate (a/h = 100).

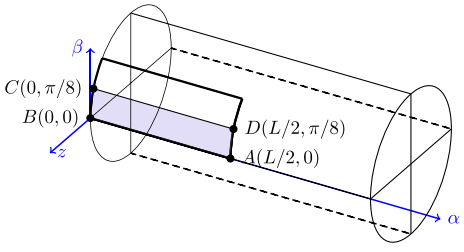

Fig. 5. Cylindrical shell.

Table 5
Convergence study. Cylindrical shell with lamination (0°/90°) and thickness ratio $a/h = 100$. LW model *SaS5* is adopted.

Mesh	$\bar{u}_z$ $(\frac{L}{2},0,0)$	$\bar{\sigma}_{\alpha\alpha}$ $(\frac{L}{2},0,\frac{h}{2})$	$\bar{\sigma}_{\alpha z}$ $(0,0,-\frac{h}{4})$	$\bar{\sigma}_{zz}$ $(\frac{L}{2},0,\frac{h}{4})$
2×4	0.1369	0.1962	−1.523	−7.764
4×8	0.1367	0.1895	−1.517	−7.783
6×12	0.1367	0.1882	−1.516	−7.749
8×16	0.1367	0.1877	−1.515	−7.734
10×20	0.1367	0.1875	−1.514	−7.726
Kulikov [61]	0.1367	0.1871	−1.512	−7.707
Varadan [75]	0.1367	0.1871	−1.512	−7.71

$$\bar{u}_z = \frac{E_L h^3}{p_0 R^4} u_z, \quad \bar{\sigma}_{\alpha\alpha} = \frac{10h^2}{p_0 R^2}\sigma_{\alpha\alpha}, \quad \bar{\sigma}_{\beta\beta} = \frac{h^2}{p_0 R^2}\sigma_{\beta\beta}, \quad \bar{\sigma}_{\alpha\beta} = \frac{100h^2}{p_0 R^2}\sigma_{\alpha\beta},$$
$$\bar{\sigma}_{\alpha z} = \frac{100h}{p_0 R}\sigma_{\alpha z}, \quad \bar{\sigma}_{\beta z} = \frac{10h}{p_0 R}\sigma_{\beta z}, \quad \bar{\sigma}_{zz} = \frac{1}{p_0}\sigma_{zz} \tag{37}$$

Table 6
Cylindrical shell with lamination (0°/90°). Results obtained with SaS and Legendre Polynomials implemented in LW approach.

R_β/h	Kinematics	$\bar{u}_z$ $(\frac{L}{2},0,0)$	$\bar{\sigma}_{\alpha\alpha}$ $(\frac{L}{2},0,\frac{h}{2})$	$\bar{\sigma}_{\alpha z}$ $(0,0,-\frac{h}{4})$	$\bar{\sigma}_{zz}$ $(\frac{L}{2},0,\frac{h}{4})$	N_{exp}
2	*LGD*1	1.254	0.0202	3.649	−0.3060	3
	*LGD*4	1.402	0.2414	4.829	−0.3174	9
	*SaS*3	1.340	0.1940	3.658	−0.3205	5
	*SaS*5	1.402	0.2414	4.829	−0.3174	9
	*SaS*7	1.403	0.2511	4.795	−0.3123	13
	Varadan [75]	1.4034	0.2511	4.786	−0.31	
100	*LGD*1	0.1364	0.2035	−1.655	−5.628	3
	*LGD*4	0.1367	0.1875	−1.514	−7.726	9
	*SaS*3	0.1367	0.1864	−1.660	−5.548	5
	*SaS*5	0.1367	0.1875	−1.514	−7.726	9
	Varadan [75]	0.1367	0.1871	−1.512	−7.71	

To reduce the computational cost, a 1/16 of the whole shell is considered (1/2 in axial and 1/8 in circumferential directions, respectively) with cyclic/symmetric boundary conditions applied on the edges. Following the same procedure used in last section, 3D stress distribution are approximated with LW models by implementing SaS and Legendre polynomials; then various ESL models based on miscellaneous series expansions are compared to the exact and SaS solutions. For SaS and ESL models, by increasing the number of expansion, convergent displacement and stress results are reached. The zig-zag function is also used to improve the continuity of transverse stresses in ESL models.

6.2.1. Convergence and locking study

In the convergence study of Table 5, the results in terms of both displacement and stresses for $a/h = 100$ and different mesh sizes are summarized and compared with both the exact solution by Varadan and Bhaskar [75] and SaS5 analytical solution by Kulikov and Plotnikova [61]. Lagrange polynomials of order 4 (5 expansion terms) and layer-wise approach, that is SaS5 model, are used.

The convergence study demonstrates that the element is stable for the analysis of thin shells and it is not affected by the membrane or shear locking and the mesh 10×20 has be chosen for the following analyses in order to ensure good convergence also for the transverse stresses.

Table 7
Thick cylindrical shell with lamination (0°/90°). Results obtained with various and miscellaneous expansions implemented in ESL approach.

R_β/h	Kinematics	$\bar{u}_z$ $(\frac{L}{2},0,0)$	$\bar{\sigma}_{\alpha\alpha}$ $(\frac{L}{2},0,\frac{h}{2})$	$\bar{\sigma}_{\alpha z}$ $(0,0,-\frac{h}{4})$	$\bar{\sigma}_{zz}$ $(\frac{L}{2},0,\frac{h}{4})$	N_{exp}
2	*FSDT*	1.222	0.2119	3.328	-	
	*ET*1	1.329	−0.0503	4.300	−0.4398	2
	*ET*3	1.359	0.2612	4.303	−0.3260	4
	*ET*5	1.382	0.2650	4.497	−0.3129	6
	*ET*8	1.388	0.2497	4.748	−0.3140	9
	ET1Z	1.316	0.02089	3.845	−0.3135	3
	ET3Z	1.385	0.2428	4.147	−0.2984	5
	ET5Z	1.389	0.2653	4.749	−0.2820	7
	ET7Z	1.396	0.2417	4.825	−0.2848	9
	*EExp*1	1.310	−0.09375	5.207	−0.4154	2
	*EExp*3	1.342	0.2355	3.655	−0.2930	4
	*EExp*5	1.369	0.2710	4.097	−0.3020	6
	*EExp*8	1.387	0.2350	4.541	−0.3103	9
	EExp1Z	1.336	−0.03850	4.017	−0.2787	3
	EExp3Z	1.376	0.2500	3.649	−0.2526	5
	EExp5Z	1.385	0.2702	4.574	−0.2653	7
	EExp8Z	1.397	0.2752	4.839	−0.2861	10
	*ES*1	1.251	0.1724	5.062	−0.3979	2
	*ES*3	1.404	0.1260	5.215	−0.4383	4
	*ES*5	1.407	0.1191	5.017	−0.4446	6
	ES1Z	1.229	0.2312	4.050	−0.2886	3
	ES3Z	1.403	0.1893	4.740	−0.2972	5
	ES5Z	1.407	0.1846	4.529	−0.3013	7
	*ES1C*1	1.183	0.2854	3.646	−0.2606	3
	*ES3C*3	1.388	0.2515	4.776	−0.3111	7
	*ES5C*5	1.393	0.2515	4.995	−0.3102	11
	ES1C1Z	1.175	0.2950	3.589	−0.2690	4
	ES3C3Z	1.394	0.2502	5.001	−0.2832	8
	ES5C5Z	1.402	0.2514	4.790	−0.2746	12
	ET1Exp1Z	1.268	0.1823	3.603	−0.3353	4
	ET1Exp3Z	1.391	0.2331	4.212	−0.2658	6
	ET1Exp5Z	1.390	0.2299	4.802	−0.2925	8
	ET1S1Z	1.375	0.1505	4.120	−0.3174	4
	ET1S3Z	1.406	0.1855	4.557	−0.3002	6
	ET1S5Z	1.407	0.1860	4.524	−0.3018	8
	Varadan [75]	1.4034	0.2511	4.786	−0.31	

Table 8
Cylindrical shell with lamination (0°/90°). Results obtained with various and miscellaneous expansions implemented in ESL approach.

R_β/h	Kinematics	$\bar{u}_z$ $(\frac{L}{2},0,0)$	$\bar{\sigma}_{\alpha\alpha}$ $(\frac{L}{2},0,\frac{h}{2})$	$\bar{\sigma}_{\alpha z}$ $(0,0,-\frac{h}{4})$	$\bar{\sigma}_{zz}$ $(\frac{L}{2},0,\frac{h}{4})$	N_{exp}
100	*FSDT*	0.1367	0.1874	−2.479	–	
	*ET*1	0.1367	0.1903	−2.483	51.10	2
	*ET*3	0.1367	0.1872	−2.452	−6.788	4
	*ET*5	0.1367	0.1871	−1.389	−5.902	6
	*ET*8	0.1367	0.1866	−1.375	−7.350	9
	ET1Z	0.1364	0.2035	−1.681	−5.664	3
	ET3Z	0.1367	0.1863	−2.187	−4.862	5
	ET5Z	0.1367	0.1880	−1.686	−7.101	7
	ET7Z	0.1367	0.1873	−1.407	−7.973	9
	*EExp*1	0.007782	0.01112	28.03	1.871	2
	*EExp*3	0.1277	0.1786	−25.66	−12.16	4
	*EExp*5	0.1367	0.1893	−2.991	−4.084	6
	*EExp*8	0.1367	0.1878	−1.123	−7.712	9
	EExp1Z	0.01695	0.02604	5.111	−1.701	3
	EExp3Z	0.1279	0.1796	−22.42	−11.92	5
	EExp5Z	0.1367	0.1884	−2.978	−6.020	7
	EExp7Z	0.1367	0.1875	−1.439	−7.894	9
	*ES*2	0.03238	0.05066	−50.63	11.45	3
	*ES*4	0.1349	0.2145	0.3057	48.94	5
	*ES*6	0.1356	0.2158	−1.981	49.57	7
	ES2Z	0.03247	0.04746	−52.22	−1.590	4
	ES4Z	0.1357	0.2015	1.185	−6.991	6
	ES6Z	0.1364	0.2027	−1.301	−6.703	8
	*ES2C*2	0.03456	0.04640	−38.73	−1.154	5
	*ES4C*4	0.1360	0.1858	−1.258	−8.155	9
	*ES6C*6	0.1367	0.1870	−1.419	−8.289	13
	ES2C2Z	0.03685	0.04969	−31.86	−0.8721	6
	ES4C4Z	0.1361	0.1864	−1.524	−7.907	10
	ES6C6Z	0.1367	0.1874	−1.325	−7.633	14
	ET1Exp2Z	0.1367	0.1870	−1.866	−5.908	5
	ET1Exp4Z	0.1367	0.1883	−1.664	−6.528	7
	ET1Exp6Z	0.1367	0.1872	−1.538	−7.815	9
	ET1S1Z	0.1364	0.2021	−2.044	−5.044	4
	ET1S2Z	0.1364	0.2031	−1.610	−6.427	5
	ET1S3Z	0.1364	0.2026	−1.399	−7.038	6
	Varadan [75]	0.1367	0.1871	−1.512	−7.71	

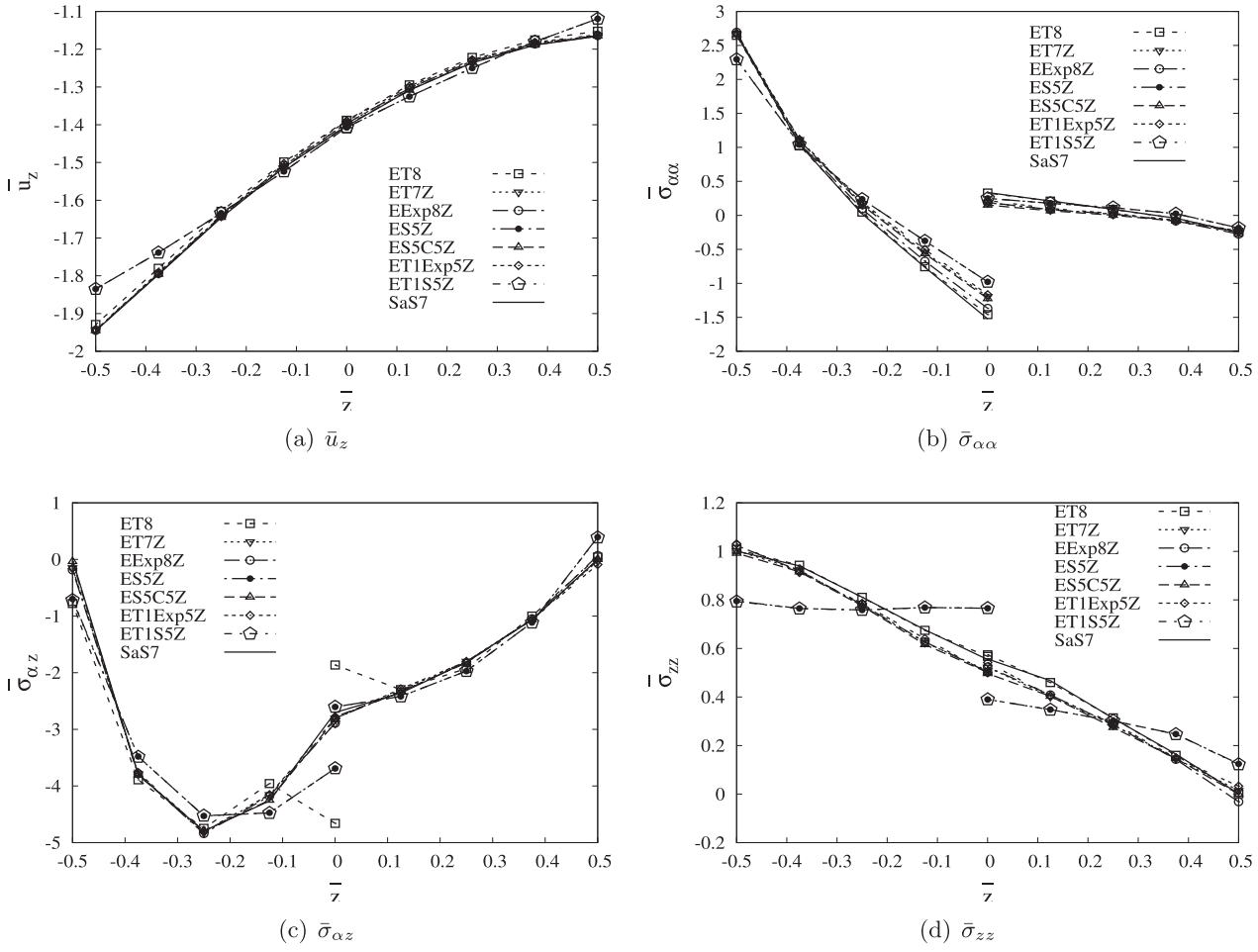

Fig. 6. Transverse displacement and stresses evaluation. Results obtained by selected kinematics, thick shell ($R_\beta/h = 2$).

6.2.2. Results obtained with SaS and Legendre expansions in LW approach

In Table 6, layer-wise results in terms of transversal displacement, in-plane stress and transverse shear and normal stress are given for thick and thin shell and compared with the solution by Varadan and Bhaskar [75]. As for the plate, both Lagrange expansion on Chebyshev nodes (SaS) and Legendre expansion (LGD) are considered, even if they provide the same values. Expansion numbers up to 7 and 5 are used for SaS models to obtain a good approximation of transverse stresses in thick and thin shells, respectively.

6.2.3. Results obtained with ESL models using various and miscellaneous expansions

In Tables 7 and 8, equivalent-single layer results for various and miscellaneous expansions are presented for the thick ($R_\beta/h = 2$) and thin ($R_\beta/h = 100$) shell, respectively. The comments to these tables are very similar to the case of the plate, although lamination is here anti-symmetric. The results are good in terms of both displacements and stresses if enough terms are considered in the models and the convergent numbers of expansion is almost the same of the plate case. It is difficult to define a general trend for exponential and sinusoidal models and oscillations can be noted in some cases, in particular for transverse stresses. The inclusion of zig-zag term helps the different theories to provide better results in terms of transverse stresses and the T1 term reduces the number of expansion required for the convergence. No particular benefits are here noted by adding the cosinusoidal terms in the trigonometric expansion; this is possible due to the anti-symmetric lay-up.

Figs. 6 and 7 represent the distributions along the thickness of transversal displacement, in-plane stress and transverse shear and normal stresses for the thick and thin shell, respectively. For each kind of expansion, the models with highest expansion number from Tables 6–8 are chosen. It is confirmed that good approximations are obtained with almost all kind of models with zig-zag function and sufficient number of expansion. The pure Taylor expansion is very far from satisfying the interlaminar continuity conditions for the transverse stresses and sinusoidal models provide very inaccurate results in terms of transverse normal stress. Unlike the plate case, the transverse normal stress is here well approximated in both thick and thin shell, but the Fig. 7(e) demonstrates that it depends on the lower number of layers: if four layers are considered (two fictitious layers with same properties for each physical layer) the discontinuity of σ_{zz} increases.

7. Conclusions

This paper has dealt with the static analysis of composite plates and shells by means of a MITC9 shell finite element, based on the Unified Formulation, with various and miscellaneous through-the-thickness kinematics. The element has been assessed by analyzing cross-ply structures with symmetric and anti-symmetric lamination under bi-sinusoidal loads and simply-supported boundary

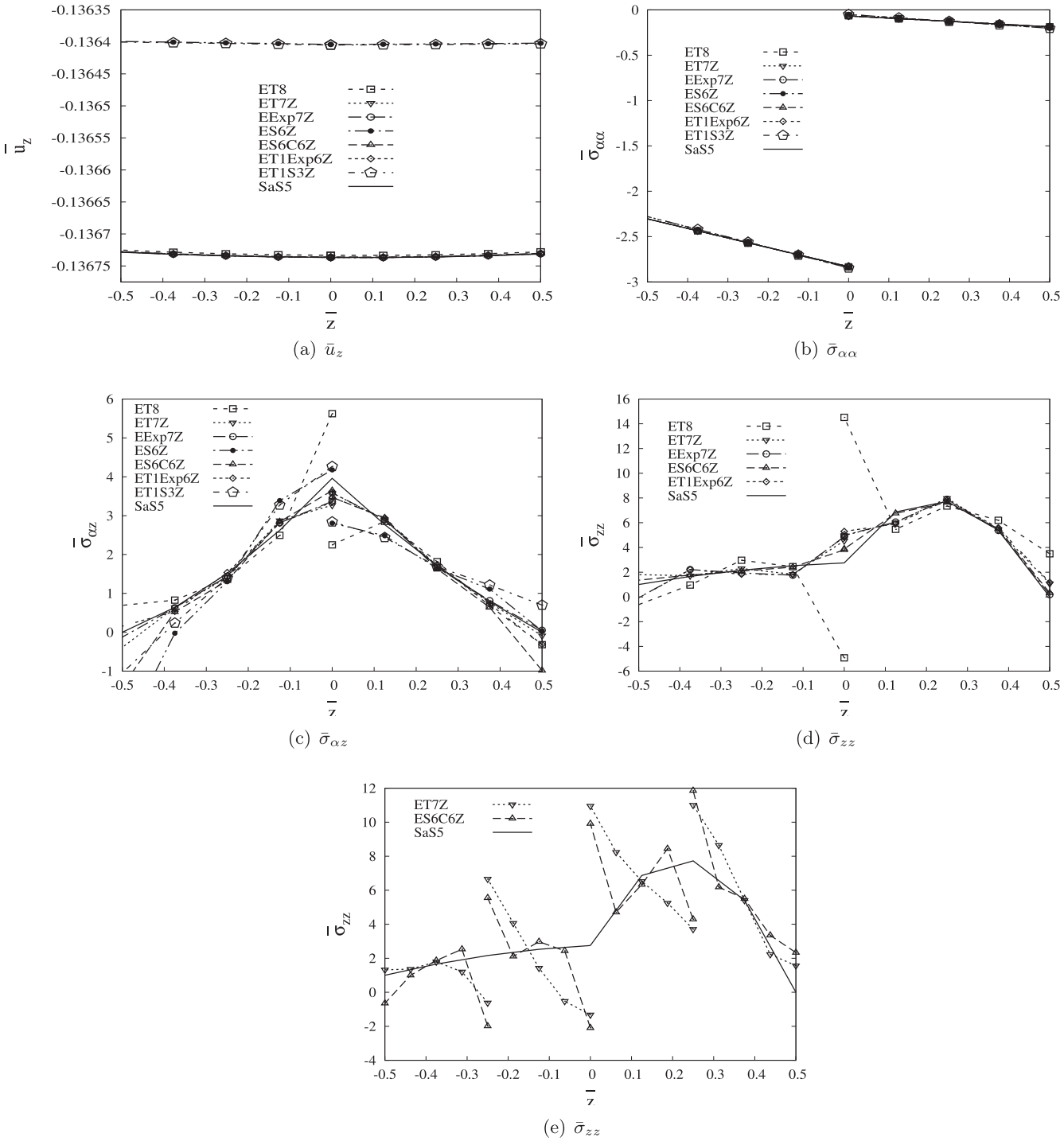

Fig. 7. Transverse displacement and stresses evaluation. Results obtained by selected kinematics, thin shell ($R_\beta/h = 100$).

conditions. The results have been presented in terms of transverse displacement, in-plane stresses, transverse shear and normal stresses for different thickness ratios. The performances of the shell element have been tested, and the different theories in both layer-wise (SaS and Legendre expansion) and equivalent-single-layer (Taylor, exponential and sinusoidal expansions with and without zig-zag function) approach have been compared. The following conclusions can be drawn:

1. by studying cross-ply thin plate and shell structures, it has been demonstrated once again that the MITC9 shell element is not affected by shear or membrane locking;
2. in the case of LW approach, it has been shown that SaS and Legendre models provide the same results if the same polynomial order is considered;
3. in the case of ESL approach, the results converge to the reference solution by increasing the number of expansion of the models, regardless of the employed function type. In few cases, some oscillations can be noted for exponential and sinusoidal models, in particular in terms of transverse stresses;
4. the number of expansion required for the convergence is slightly reduced in the case of sinusoidal models but the results obtained are not enough accurate in respect to the reference solution;

5. the approximation of transverse stresses is very inaccurate in both thick plate and shell for the ESL models;
6. the exponential series expansions lead to good results for all the study cases, even if the convergence number of expansion is almost the same of the Taylor expansions.
7. some benefits are given by the addition of cosinusoidal terms in the trigonometric series expansions if the anti-symmetric lamination is considered, but this implicates a significant increase of the expansion number;
8. the zig-zag function is fundamental for the description of the transverse stresses along the thickness independently of the thickness ratio. Only in the case of sinusoidal models, the inclusion of zig-zag term doesn't produce notable improvements in the transverse stresses, less among them the transverse normal stress;
9. for comparable numbers of expansion, the exponential and sinusoidal models provide worse results than FSDT;
10. the combination of the linear Taylor term with the trigonometric and exponential series is very important for the reduction of the terms required to reach the convergence;
11. if thin structures with high number of layers are studied, ESL theories are not able to approximate the continuity of the transverse normal stress, even including the zig-zag term.

Starting from this paper, future companion works can be devoted to the asymptotic analysis of the 'best' models with miscellaneous kinematics to be used for the study of composite plates and shells. For further details about the asymptotic analysis the reader can refer to the works [76–80].

Acknowledgements

The work of the first and forth authors was supported by the Russian Science Foundation (Grant No. 15-19-30002).

References

[1] Argyris JH. Matrix displacement analysis of plates and shells, prolegomena to a general theory, Part I. Ingeniur-Archiv 1966;35:102–42.
[2] Sabir AB, Lock AC. The application of finite elements to the large deflection geometrically non-linear behaviour of cylindrical shells. In: Brebbia CA, Tottenham H, editors. Variational methods in engineering, vol. 2. Southampton University Press; 1972 (7/66–7/75).
[3] Wempner GA, Oden JT, Kross DA. Finite element analysis of thin shells. J Eng Mech ASCE 94 1968;94:1273–94.
[4] Abel JF, Popov EP. Static and dynamic finite element analysis of sandwich structures. Proceedings of the second conference of matrix methods in structural mechanics, vol. AFFSL-TR-68-150. p. 213–45.
[5] Monforton GR, Schmidt LA. Finite element analyses of sandwich plates and cylindrical shells with laminated faces. In: Proceedings of the second conference of matrix methods in structural mechanics. vol. AFFSL-TR-68-150. p. 573-308.
[6] Pryor CW, Barker RM. A finite element analysis including transverse shear effect for applications to laminated plates. Am Inst Aeronaut Astronaut J 1971;9:912–7.
[7] Noor AK. Finite element analysis of anisotropic plates. Am Inst Aeronaut Astronaut J 1972;11:289–307.
[8] Hughes TJR, Tezduyar T. Finite elements based upon Mindlin plate theory with particular reference to the four-node isoparametric element. J Appl Mech 1981;48:587–96.
[9] Panda SC, Natarajan R. Finite element analysis of laminated composites plates. Int J Numer Meth Eng 1979;14:69–79.
[10] Parisch H. A critical survey of the 9-node degenerated shell element with special emphasis on thin shell application and reduced integration. Comput Methods Appl Mech Eng 1979;20:323–50.
[11] Ferreira AJM, Barbosa JT, Marques AT, De Sá JC. Non-linear analysis of sandwich shells: the effect of core plasticity. Comput Struct 2000;76:337–46.
[12] Kant T, Owen DRJ, Zienkiewicz OC. Refined higher order C^0 plate bending element. Comput Struct 1982;15:177–83.
[13] Kant T, Kommineni JR. Large amplitude free vibration analysis of cross-ply composite and sandwich laminates with a refined theory and C0 finite elements. Comput Struct 1989;50:123–34.
[14] Dau F, Polit O, Touratier M. C^1 plate and shell finite elements for geometrically nonlinear analysis of multilayered structures. Comput Struct 2006;84:1264–74.
[15] Dau F, Polit O, Touratier M. An efficient C^1 finite element with continuity requirements for multilayered/sandwich shell structures. Comput Struct 2004;82:1889–99.
[16] Polit O, Touratier M. A multilayered/sandwich triangular finite element applied to linear and non-linear analyses. Compos Struct 2002;58:121–8.
[17] Polit O, Touratier M. High-order triangular sandwich plate finite element for linear and non-linear analyses. Comput Methods Appl Mech Eng 2000;185:305–24.
[18] Polit O, Touratier M. A new laminated triangular finite element assuring interface continuity for displacements and stresses. Compos Struct 1997;38(1-4):37–44.
[19] Tessler A. A Higher-order plate theory with ideal finite element suitability. Comput Methods Appl Mech Eng 1991;85:183–205.
[20] Reddy JN. Mechanics of laminated composite plates and shells, theory and analysis. CRC Press; 1997.
[21] Palazotto AN, Dennis ST. Nonlinear analysis of shell structures. AIAA Series. Springer; 1992.
[22] Disciuva M, Cicorello A, Dalle Mura E. A class of multilayered anisotropic plate elements including the effects of transverse shear deformabilty. In: Proceedings of AIDAA conference, Torino. p. 877–92.
[23] Bekou A, Touratier M. A rectangular finite element for analysis composite multilayerd shallow shells in static, vibration and buckling. Int J Numer Meth Eng 1993;36:627–53.
[24] Reissner E. On a certain mixed variational theorem and on laminated elastic shell theory. Proce Euromech-Colloquium 1986;219:17–27.
[25] Rao KM, Meyer-Piening HR. Analysis of thick laminated anisotropic composites plates by the finite element method. Compos Struct 1990;15:185–213.
[26] Carrera E. A class of two-dimensional theories for anisotropic multilayered plates analysis. In: Accademia delle Scienze di Torino, Memorie Scienze Fisiche, 1995-1996. p. 19–20. p. 1–39.
[27] Murakami H. Laminated composite plate theory with improved in-plane responses. J Appl Mech 1986;53:661–6.
[28] Brank B, Carrera E. Multilayered shell finite element with interlaminar continuous shear stresses: a refinement of the Reissner-Mindlin formulation. Int J Numer Meth Eng 2000;48:843–74.
[29] Shimpi RP, Ghugal YM. A new layerwise trigonometric shear deformation theory for two-layered cross-ply beams. Compos Sci Technol 2001;61(9):1271–83.
[30] Arya H, Shimpi RP, Naik NK. A zigzag model for laminated composite beams. Compos Struct 2002;56:21–4.
[31] Ferreira AJM, Roque CMC, Jorge RMN. Analysis of composite plates by trigonometric shear deformation theory and multiquadrics. Comput Struct 2005;83(27):2225–37.
[32] Roque CMC, Ferreira AJM, Jorge RMN. Modelling of composite and sandwich plates by a trigonometric layerwise deformation theory and radial basis functions. Compos Part B 2005;36(8):559–72.
[33] Vidal P, Polit O. A family of sinus finite elements for the analysis of rectangular laminated beams. Compos Struct 2008;84:56–72.
[34] Vidal P, Polit O. A sine finite element using a zig-zag function for the analysis of laminated composite beams. Compos Part B 2011;42(6):1671–82.
[35] Ferreira AJM, Carrera E, Cinefra M, Roque CMC, Polit O. Analysis of laminated shells by a sinusoidal shear deformation theory and radial basis functions collocation, accounting for through-the-thickness deformations. Compos Part B 2011;42(5):1276–84.
[36] Mantari JL, Bonilla EM, Guedes Soares C. A new tangential-exponential higher order shear deformation theory for advanced composite plates. Compos Part B 2014;60:319–28.
[37] Mantari JL, Oktem AS, Guedes Soares C. Bending response of functionally graded plates by using a new higher order shear deformation theory. Compos Struct 2012;94:714–23.
[38] Mantari JL, Oktem AS, Guedes Soares C. Static and dynamic analysis of laminated composite and sandwich plates and shells by using a new higher-order shear deformation theory. Compos Struct 2011;94:37–49.
[39] Mantari JL, Oktem AS, Guedes Soares C. A new trigonometric deformation theory for isotropic, laminated composite and sandwich plates. Int J Solids Struct 2012;49:43–53.
[40] Karama M, Afaq KS, Mistou S. Mechanical behaviour of laminated composite beam by the new multi-layered laminated composite structure model with transverse shear stress continuity. Int J Solids Struct 2003;40:1525–46.
[41] Karama M, Afaq KS, Mistou S. A refinement of Ambartsumian multi-layer beam theory. Compos Struct 2008;86:839–49.
[42] Aydogdu M. A new shear deformation theory for laminated composite plates. Compos Struct 2009;89:94–101.
[43] Carrera E, Filippi M, Zappino E. Laminated beam analysis by polynomial, trigonometric, exponential and zig-zag theories. Eur J Mech A Solids 2013;41:58–69.
[44] Carrera E, Filippi M, Zappino E. Free vibration analysis of laminated beam by polynomial, trigonometric, exponential and zig-zag theories. J Compos Mater 2014;48(19):2299–316.
[45] Filippi M, Petrolo M, Valvano S, Carrera E. Analysis of laminated composites and sandwich structures by trigonometric, exponential and miscellaneous polynomials and a MITC9 plate element. Compos Struct 2016;150:103–14.
[46] Carrera E. Theories and finite elements for multilayered anisotropic composite plates and shells. Arch Comput Methods Eng 2002;9:87–140.

[47] Carrera E. Theories and finite elements for multilayered plates and shells: a unified compact formulation with numerical assessment and benchmarking. Arch Comput Methods Eng 2003;10(3):215–96.
[48] Cinefra M, Chinosi C, Della Croce L. MITC9 shell elements based on refined theories for the analysis of isotropic cylindrical structures. Mech Adv Mater Struct 2013;20:91–100.
[49] Bathe KJ, Lee PS, Hiller JF. Towards improving the MITC9 shell element. Comput Struct 2003;81:477–89.
[50] Chinosi C, Della Croce L. Mixed-interpolated elements for thin shell. Commun Numer Methods Eng 1998;14:1155–70.
[51] Huang NC. Membrane locking and assumed strain shell elements. Comput Struct 1987;27(5):671–7.
[52] Panasz P, Wisniewski K. Nine-node shell elements with 6 dofs/node based on two-level approximations. Part I: theory and linear tests. Finite Elem Anal Des 2008;44:784–96.
[53] Noor AK, Burton WS. Assessment of computational models for multi-layered composite shells. Appl Mech Rev 1990;43:67–97.
[54] Reddy JN. An evaluation of equivalent single layer and layer-wise theories of composite laminates. Compos Struct 1993;25:21–35.
[55] Mawenya AS, Davies JD. Finite element bending analysis of multilayer plates. Int J Numer Meth Eng 1974;8:215–25.
[56] Pinsky PM, Kim KO. A multi-director formulation for nonlinear elastic-viscoelastic layered shells. Comput Struct 1986;24:901–13.
[57] Chaudhuri RA, Seide P. An approximate method for prediction of transverse shear stresses in a laminated shell. Int J Solids Struct 1987;23:1145–61.
[58] Rammerstorfer FG, Dorninger K, Starlinger A. Composite and sandwich shells. in [388]; 1992, p. 131–94.
[59] Cinefra M, Carrera E. Shell finite elements with different through-the-thickness kinematics for the linear analysis of cylindrical multilayered structures. Int J Numer Meth Eng 2013;93:160–82.
[60] Kulikov GM, Plotnikova SV. Exact 3D stress analysis of laminated composite plates by sampling surfaces method. Compos Struct 2012;94(12):3654–63.
[61] Kulikov GM, Plotnikova SV. Advanced formulation for laminated composite shells: 3D stress analysis and rigid-body motions. Compos Struct 2013;95:236–46.
[62] Kulikov GM, Plotnikova SV. Hybrid-mixed ANS finite elements for stress analysis of laminated composite structures: sampling surfaces plate formulation. Comput Methods Appl Mech Eng 2016;303:374–99.
[63] Kulikov GM. Refined global approximation theory of multilayered plates and shells. J Eng Mech 2001;127:119–25.
[64] Kulikov GM, Carrera E. Finite deformation higher-order shell models and rigid-body motions. Int J Solids Struct 2008;45:3153–72.
[65] Naghdi PM. The theory of shells and plates. Handbuch der Physic, vol. 4. Berlin: Springer; 1972. p. 425–640.
[66] Koiter WT. On the foundations of the linear theory of thin elastic shell. Proc Kon Nederl Akad Wetensch 1970;73:169–95.
[67] Ciarlet PG, Gratie L. Another approach to linear shell theory and a new proof of Korn's inequality on a surface. C R Acad Sci Paris Ser I 2005;340:471–8.
[68] Murakami H. Laminated composite plate theory with improved in-plane responses. J Appl Mech 1986;53:661–6.
[69] Cinefra M, Valvano S. A variable kinematic doubly-curved MITC9 shell element for the analysis of laminated composites. Mech Adv Mater Struct 2016;23(11):1312–25.
[70] Rogacheva NN. The theory of piezoelectric Shells and Plates. Boca Raton, Florida (USA): CRC Press; 1994.
[71] Chapelle D, Bathe KJ. The finite element analysis of shells – fundamentals. Berlin: Springer; 2003.
[72] Bathe K-J, Dvorkin E. A formulation of general shell elements – the use of mixed interpolation of tensorial components. Int J Numer Meth Eng 1986;22:697–722.
[73] Bucalem ML, Bathe K-J. Higher-order MITC general shell elements. Int J Numer Meth Eng 1993;36:3729–54.
[74] Pagano NJ. Exact solutions for rectangular bidirectional composites and sandwich plates. J Compos Mater 1970;4:20–34.
[75] Varadan TK, Bhaskar K. Bending of laminated orthotropic cylindrical shells — an elasticity approach. Compos Struct 1991;17(2):141–56.
[76] Carrera E, Petrolo M. Guidelines and recommendation to construct theories for metallic and composite plates. AIAA J 2010;48(12):2852–66.
[77] Carrera E, Miglioretti F, Petrolo M. Guidelines and recommendations on the use of higher order finite elements for bending analysis of plates. Int J Comput Methods Eng Sci Mech 2011;12(6):303–24.
[78] Petrolo M, Miglioretti F. Selection of appropriate multilayered plate theories by using a genetic like algorithm. Compos Struct 2012;94(3):1175–86.
[79] Carrera E, Cinefra M, Lamberti A, Petrolo M. Results on best theories for metallic and laminated shells including layer-wise models. Compos Struct 2015;126:285–98.
[80] Cinefra M, Lamberti A, Zenkour AM, Carrera E. Axiomatic/asymptotic technique applied to refined theories for piezoelectric plates. SMART2013 – special issue of Mech Adv Mater Struct 2015;22:107–24.